Polymer lattice-reinforcement for enhancing ductility of concrete

Brian Salazar[a1], Parham Aghdasi[b], Ian D. Williams[b], Claudia P. Ostertag[b], Hayden K. Taylor[a1]

[a] Department of Mechanical Engineering, University of California, Berkeley, Berkeley, CA, USA

[b] Department of Civil and Environmental Engineering, University of California, Berkeley, Berkeley, CA, USA

Keywords: Three-dimensional reinforcement, Mechanical Properties, Lattice-reinforcement, Polymeric reinforcement, Concrete

Highlights

- Ultra-high-performance concrete was reinforced with 3D-printed, stretch-dominated polymeric lattices, resulting in greatly increased ductility
- Ductility was optimized by deliberately orienting 3D printed polymer filaments in line with the expected tensile stresses.
- The ductility-enhancing mechanisms during flexure are associated with multiple cracking and tortuous crack paths.
- This fabrication method allows easy pouring of the mortar mixture, unlike polymer fiber-reinforced composites.

[1] Corresponding authors. Email addresses: brian10salazar@berkeley.edu (B. Salazar); hkt@berkeley.edu (H. Taylor)

- This composite production method lends itself more readily to automated manufacturing than conventional steel rebar-reinforced concrete.

Graphical abstract

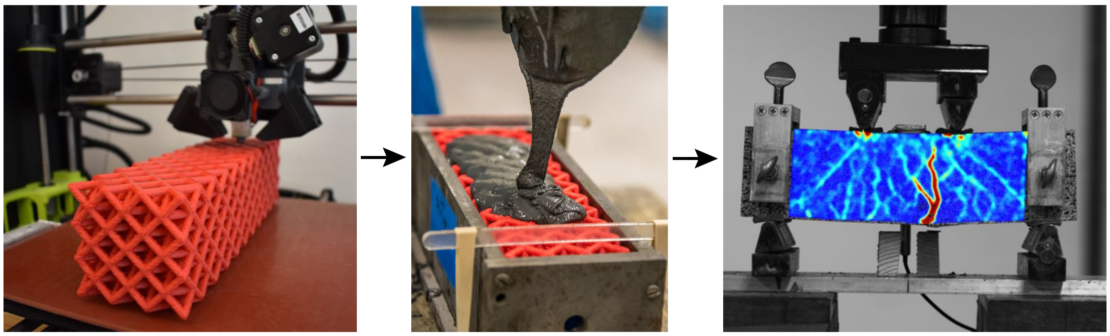

Abstract

Concrete is the most widely used engineering material. While strong in compression, concrete is weak in tension and exhibits low ductility due to its low crack growth resistance. With increasing compressive strength, concrete becomes even more brittle, hence requiring appropriate reinforcement to enhance its ductility. This paper presents a new method for increasing the ductility of ultra-high-performance concrete by reinforcing it with 3D printed polymeric lattices made of either polylactic acid (PLA) or acrylonitrile butadiene styrene (ABS). These lattice-reinforced concrete specimens were then tested in compression and four-point bending. The effect of polymeric reinforcement ratios on mechanical properties was investigated by testing two lattice configurations. The lattices were very successful in transforming the brittle ultra-high-performance concrete (UHPC) into a ductile material with strain hardening behavior; all flexural specimens revealed multiple cracking and strain hardening behavior up to peak load. Increasing the ABS reinforcing ratio from 19.2% to 33.7% resulted in a 22% reduction in average compressive strength. However, in flexure, increasing the PLA reinforcing ratio from 19.2% to 33.7% resulted in a 38% increase in average peak load. The compression results of all

specimens independent of their reinforcement ratio revealed smooth softening behavior in compression.

1. Introduction

Concrete strikes a balance between performance, cost, and availability. It has enabled many of the largest and most demanding engineering projects in the world, and also finds its place in less grandiose projects such as home foundations and sidewalks. On its own, the brittle tensile response and quasi-brittle compressive response of concrete would limit its usefulness to simple, compression-only load cases. As such, it relies on the composite behavior provided by the reinforcement to provide ductile, predictable response under many types of loading demands.

Steel rebar cages are traditionally used to provide the requisite reinforcement and can be detailed to effectively resist certain load cases — but they also come with limitations. As structural elements trend toward more slender beams and columns using higher strength concrete, conventional reinforcement detailing may not be enough to resist large demands such as seismic or blast loading. Furthermore, rebar cages with high reinforcing bar ratios are not only very labor-intensive to construct but also difficult to infiltrate with concrete.

An alternative way to enhance the ductility of concrete is through the use of discrete steel or polymer fibers. However, the fiber distribution in fiber-reinforced concrete composites cannot be easily controlled, hence leaving sections for the cracks to propagate uninhibited [1–6]. This heterogeneity leads to unpredictability in the overall performance of fiber reinforced composites and can reduce the expected tensile strength and fracture toughness of the material [7]. The continuity and predictability inherent to three-dimensional reinforcements could potentially be the key to mitigating these issues.

Textile reinforced concrete (TRC) uses a similar principle, but in two dimensions, and has been shown to provide excellent reinforcement. Being reinforced in only two dimensions, however, TRCs have limited usefulness in structural applications, and are mainly used in repair and in lightweight sandwich panels [8–15].

This paper investigates a new class of composites that utilizes three-dimensional lattice structures as reinforcements to enhance the ductility of concrete. Here, we employ the octet-truss geometry because it is known for its high specific stiffness and fracture toughness [16,17]. The octet lattices were prototyped in acrylonitrile butadiene styrene (ABS) and/or polylactic acid (PLA) using Fused Deposition Modeling (FDM) 3D printers. The use of a polymeric reinforcement material — instead of a steel reinforcement — enables the polymer-reinforced structures to be more lightweight, corrosion-resistant, and thermally insulating.

Previous research has used 3D printed polymers to reinforce cementitious material. The present authors [18] provided the first investigation of three-dimensional octet lattice-reinforced cementitious materials and found increased ductility while using a highly workable mortar. Farina et al. reinforced cement mortar with polymeric 'fibers' — in the form of simple, discrete 7.5 mm-diameter cylindrical bars — that were 3D printed from a photopolymer resin [19]. They found that augmenting the surfaces of the printed reinforcement cylinders with mm-scale protrusions led to much greater strain hardening of the composite than did smooth reinforcement rods of the same diameter and material. Samples with roughened reinforcement showed shear failure under three-point bend tests, whereas structures reinforced with smoother cylinders exhibited flexural failure. Nam et al., meanwhile, investigated the effects of reinforcement orientation and distribution by 3D printing reinforcement networks of connected photopolymer resin fibers with varying spatial distributions. They found some evidence of higher peak bending strength when using a triangulated reinforcement structure whose mesh was denser in regions of higher tensile stress [20]. However, the inherent brittleness of the cement was not significantly mitigated in any of the specimens, possibly because of the relatively low volume fraction of polymer reinforcement used.

Recently, Rosewitz et al. developed bio-inspired cement–polymer composites, and evaluated a variety of cellular polymeric reinforcement structures which showed increased ductility and, in some cases, higher peak strength than unreinforced mortar [21]. Xu et al. [22] tested the performance of thin panels reinforced with honeycomb lattices manufactured in ABS using FDM. Their panels demonstrated ductility and multiple cracking when tested in flexure. Both Rosewitz's and Xu's work, however, used prismatic or "two-dimensional" reinforcement geometries, which may limit their applicability to complex geometries or loading states.

Previous work, then, has shown the great potential of polymeric reinforcement, but highlighted several areas where further work was needed before widespread adoption. Firstly, a systematic means of incorporating fully 3D — as opposed to prismatic or 2D — reinforcement is needed, to accommodate potentially complex cast geometries and loading requirements. Secondly, the specific polymeric materials and printing method need to offer a plausible route towards scaling up the process. To this end, extrusion of thermoplastic polymers offers a more realistic prospect of large-scale production than the use of photopolymers, which tend to be much more expensive than commodity thermoplastics per unit mass. Moreover, thermoplastic extrusion can be scaled up by increasing nozzle diameter and using robotic printers, whereas photopolymer deposition rates and printing volumes remain more limited, in spite of recent progress.

The study presented here expands significantly upon our original demonstration of polymeric lattice reinforcement [18] by providing more comprehensive data on the effect of three-dimensional octet lattices on the mechanical performance of concrete. Crucially, whereas the previous study used a conventional mortar, this study concentrates on reinforcement of an ultra-high-performance-concrete (UHPC) which has previously been developed by some of the present authors [23–26]. Polymer lattice reinforcement of UHPC would be particularly advantageous: because of the advanced mortar's higher cost of production, optimized reinforcement geometries that can limit the amount of mortar used in a particular application would significantly expand its potential uses. Moreover, one of the objectives of UHPC in the first place is to reduce the amount of cement and associated CO_2 emissions required for a given load, and using a reinforcement strategy in which a significant volume fraction is *non*-cementitious can compound this advantage. Such a strategy is shown in this work, with polymeric volume fractions exceeding 30% in some cases. The polymeric phase could in principle be made from recycled material, cutting the carbon footprint further.

UHPC is, however, far more brittle than normal concrete, and hence may be expected to interact mechanically with the reinforcement in different ways and to be more difficult to enhance in ductility. It is therefore important to study whether the same degree of ductility enhancement can be achieved in UHPC as in conventional mortar, and with what degree, if any, of peak strength loss.

In this paper, we show how UHPC's ductility can be successfully increased with 3D reinforcement lattices printed from PLA or ABS, which are widely used in additive manufacturing and are available at reasonable cost. ABS is certainly already used for concrete reinforcement — for example, the carbon fiber-reinforced ABS in the "C-Fab" process marketed by Branch Technology [27]. For very high production volumes and rates, lattices could potentially be manufactured using other processes, including modified molding or casting processes. Additionally, while in this work we explore geometrically regular 3D lattices, there is the potential to spatially vary the lattice parameters — such as the polymer volume fraction — to accommodate complex loading conditions. It may even be possible to localize reinforcement material in regions where tensile loads are predicted, thereby optimizing the use of polymeric material.

2. Materials and methods

2.1 Octet lattice design

Two configurations of octet lattices were fabricated as reinforcements for the ultra-high-performance concrete: one with a low volume reinforcement ratio (19.2%) and one with a high volume reinforcement ratio (33.7%). The higher reinforcement of 33.7% was achieved by increasing the member diameter of the octet unit cells, as shown in Figure 1. The member diameters were chosen to ensure that they were several times greater than the extrusion nozzle diameter of the 3D printer used (nozzle diameters were 1.2 mm for the flexural specimens and 0.4 mm for the compressive specimens), meaning that the octet geometry could be resolved accurately and repeatably by the printer. The unit cell lengths of 11.7 and 23.5 mm were selected to be large enough that the cement mix could flow easily through the interstices of the lattice, and yet small enough that multiple unit cells could be incorporated into a sample that could be printed in a reasonable time and whose size was manageable for testing. The member diameter and unit cell lengths in turn determined the lattice volume fractions.

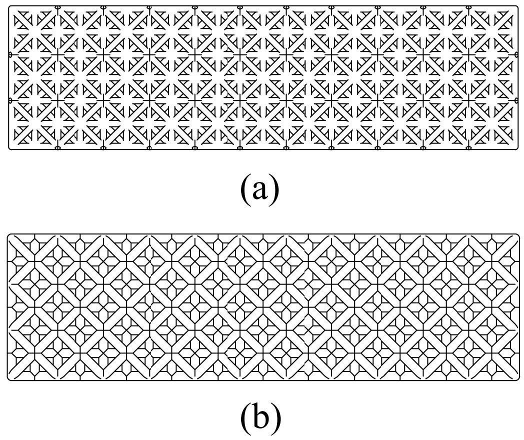

Figure 1 – the two octet lattice designs. (a) 19.2% volume fraction and (b) 33.7% volume fraction. The lattice in (b) has thicker members, and thus a higher volume fraction than (a).

Cube and beam shaped lattices as shown in Figure 2 were 3D printed. These lattices were then infiltrated with an ultra-high-performance concrete and tested in compression and four-point bending, respectively. The specimens' dimensions were chosen so that there were at least three unit cells in any direction, and are given in Table 1.

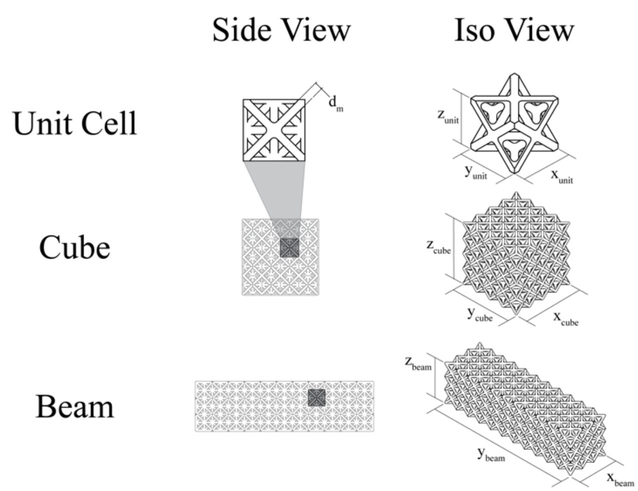

Figure 2 - Cube and beam lattice specimen descriptions

Table 1 - Geometry description for compression cube and flexural beam specimens

Specimen description	**Member diameter, d_m (mm)**	**Lattice bounding dimensions (mm^3)**	**Lattice-reinforced concrete bounding dimensions (mm^3)**	**Number of lattice unit cells across**	**Unit cell length, x_{unit} (mm)**

Compression cubes	19.2% design	1.6	48.5 × 48.5 × 48.5	50.8 × 50.8 × 50.8	4 × 4 × 4	11.7
	33.7% design	2.3	49.3 × 49.3 × 49.3			
Flexural beams	19.2% design	3.2	73.6 × 73.6 × 261.3	76.2 × 76.2 × 279.4	3 × 3 × 11	23.5
	33.7% design	4.6	74.9 × 74.9 × 262.8			

While the octet's volume percentages remained the same for compressive and flexural specimens, the scale of the octet structure changed. The octets are doubled in scale for flexural specimens compared to the compressive specimens; the octet member diameters and unit cell lengths are listed in Table 1.

2.2 Fabrication

The lattice prisms for the flexure tests were 3D printed with PLA on a LulzBot TAZ 6 machine using a 1.2 mm diameter nozzle, as shown in Figure 3a. The 1.2 mm diameter nozzle is rather coarse, which allows each beam to be printed in less than 24 hours. The thermomechanical properties of PLA allowed these lattices to be printed without any support structures. To fabricate the compression cubes from PLA, a BCN3D Sigma with a 0.4 mm nozzle diameter was used which also did not require any support material. The ABS cube lattices were produced using a Stratasys Dimension 1200es with T16 model tip using Stratasys ABSPlus model material and Stratasys P400SR support material. After printing, the support material was dissolved in an ultrasonic bath of 2% concentration sodium hydroxide (Stratasys WaterWorks).

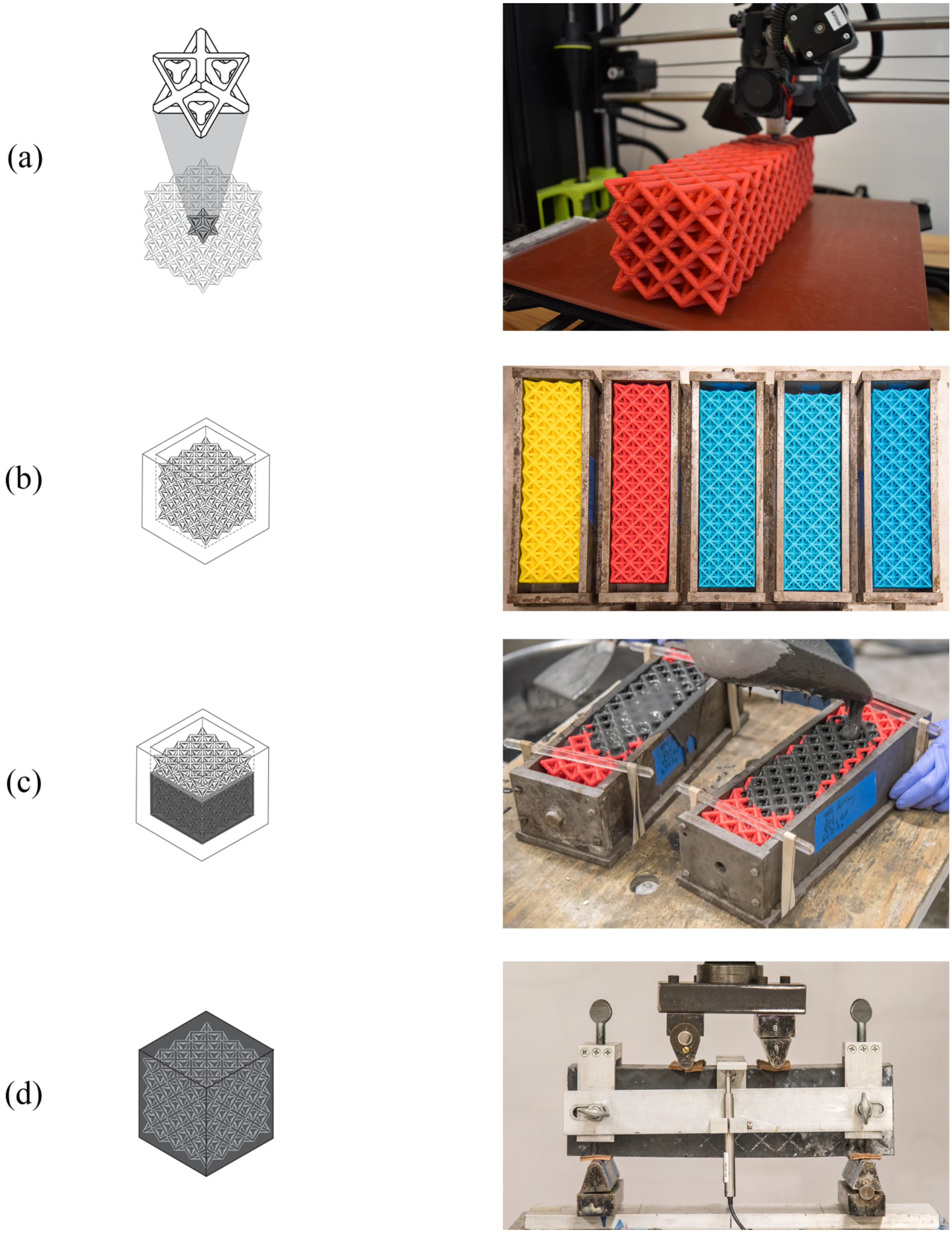

Figure 3 - Fabrication of lattice-reinforced concrete beams. (a) 3D printing of the polymeric lattice, (b) placement of lattices of different reinforcing ratios inside molds, (c) infiltration of the lattices by an ultra-high-performance concrete, and (d) cured beam ready to be tested.

Both cube and prism lattices were infiltrated with an ultra-high-performance concrete; the UHPC's weight proportions are listed in Table 2. The 7-day compressive strength of a similar UHPC is 119 MPa; further information on the UHPC mixture, development, and mechanical properties may be found in [23–26]. To create lattice-reinforced concrete beams, the lattices were placed into molds (Figure 3b), and the lattices' orientations were controlled so that the flexural tests' loading direction was aligned with the printer's build direction. Having the tension in the specimens aligned with the printed filaments ensures optimal mechanical properties. The lattices were then infiltrated with UHPC (Figure 3c), and a vibration table was used to assist with the infiltration. The addition of fly ash and superplasticizer resulted in a highly workable concrete, which allowed each lattice to be fully infiltrated. The same procedure was followed to cast lattice-reinforced concrete cubes.

The performance of the lattice-reinforced specimens is compared to a plain UHPC beam and an ultra-high-performance fiber-reinforced concrete (UHPFRC) beam reinforced with 1.4% PLA fibers (6 mm length, 1.3 denier per filament). Note that 1.4% by volume of fibers was the highest volume percent that could be incorporated into the UHPC mix while still allowing the mix to be workable enough to cast a rectangular beam.

All beams and cube specimens were stored and cured in a fog room (with 95% relative humidity at room temperature) before testing on day 7.

Table 2 - Weight proportions for the ultra-high-performance concrete mix

Ingredient	Weight proportion
Cement	1.0
Fly ash	0.1
Water	0.26
Superplasticizer	0.02
Silica sand 1 (460 µm)	0.6
Silica sand 2 (120 µm)	0.3
Glass powder	0.25
Silica fume	0.25

2.3 Uniaxial compression and four-point flexural tests

Mechanical testing was carried out on a Universal Testing Machine with a 530 kN load cell. The eight compression tests were performed according to ASTM C109 [28]. The nine beam specimens were tested in four-point bending according to ASTM C1609 [29] with a 22.9 cm span length. For both compression and flexural tests, the displacements were measured with two linear variable differential transformers (LVDTs) — one at the front of the specimens, and one at the back — and the measurements were averaged to compute the midspan deflection. On one of the 19.2% lattice-reinforced beams, and one of the 33.7% lattice-reinforced beams, a digital image correlation (DIC) technique was utilized instead of a second LVDT. For these two beams, spackle patterns (black dots on a white background) were spray-painted onto the front side and a Canon EOS 6D camera with a 100 mm macro lens then captured the displacement on the front side. The midspan deflection was then determined by averaging the displacement measured with DIC and the displacement measured with the LVDT.

3. Results and discussion

3.1 Uniaxial compression results

The lattice-reinforced UHPC's uniaxial compression results and the number of specimens tested are given in Table 3. Both the PLA and ABS lattice-reinforced cubes exhibit a lower compressive strength at the higher reinforcement percentage of 33.7% than at 19.2% polymer volume fraction. While only one PLA specimen was tested for each reinforcing ratio, the results suggest a common trend with the ABS results, whereby an increase in reinforcing ratio from 19.2% to 33.7% leads to a reduction in compressive strength. The smaller volume of UHPC at 33.7% lattice-reinforcement is responsible for the strength reduction since less of the high compressive-modulus UHPC is being incorporated into these lattices. A large reduction in strength was observed with the 33.7% ABS lattice-reinforced cubes. Both the 19.2% and 33.7% ABS lattice-reinforced cubes show high strains at the peak stress, as well as high strain energy densities. The 95% confidence intervals for the mean strain energy densities overlap for the 19.2% and 33.7% ABS-reinforced specimens.

Table 3 - Description and results of uniaxial compression tests. Values indicate 95% confidence intervals of the mean.

Cube description	**Compressive strength (MPa)**	**Strain at peak stress (mm/mm)**	**Strain energy density (MPa)**
19.2% PLA lattice-reinforcement (N = 1)	45.3	0.0114	1.86
33.7% PLA lattice-reinforcement (N = 1)	43.4	0.0161	2.09
19.2% ABS lattice-reinforcement (N = 3)	49.0 ± 1.0	0.0079 ± 0.0005	1.94 ± 0.13
33.7% ABS lattice-reinforcement (N = 3)	38.3 ± 6.0	0.0116 ± 0.0036	1.88 ± 0.32

N = number of specimens

Figure 4 shows the compressive stress–strain curves for the two types of reinforcement ratios: three curves for the 19.2% ABS lattice-reinforced UHPC cubes, and three curves for the 33.7% ABS lattice-reinforced UHPC cubes.

The concrete cubes with the larger amount of reinforcement exhibit a larger variability in stress–strain behavior, as shown by both Figure 4 and by the 95% confidence intervals for the compressive strength shown in Table 3. The larger variability in the 33.7% lattices may be caused by their smaller openings compared to the 19.2% lattices, which makes their infiltration with UHPC more difficult and hence less uniform (due to possible air voids). On the other hand, these composites exhibit smooth softening behavior up to high strain levels. In comparison, UHPC (not shown here) does not exhibit softening behavior due to its high brittleness.

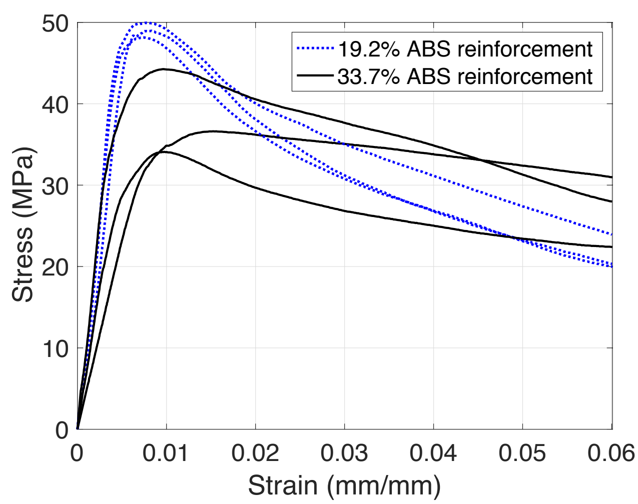

Figure 4 - Compressive stress-strain curves for ABS lattice-reinforced UHPC with 19.2% reinforcement and 33.7% reinforcement.

The compressive stress-strain curves for both ABS and PLA lattice-reinforced UHPC at 19.2% and 33.7% reinforcement, respectively, are shown in Figure 5. At both reinforcement ratios, the ABS and PLA lattice-reinforced samples perform similarly, as they exhibit similar compressive strengths and strain energy densities. From these results, it appears that PLA-reinforced UHPC may reach a higher strain at peak energy than ABS reinforced UHPC, but the overall stress–strain curve characteristics are highly similar, and more tests need to be conducted to form statistical conclusions. Figure 5 also shows the compressive behavior of the ABS lattices (without UHPC), and while both the 19.2% and 33.7% ABS lattices exhibit high ductility, they also exhibit low compressive strengths.

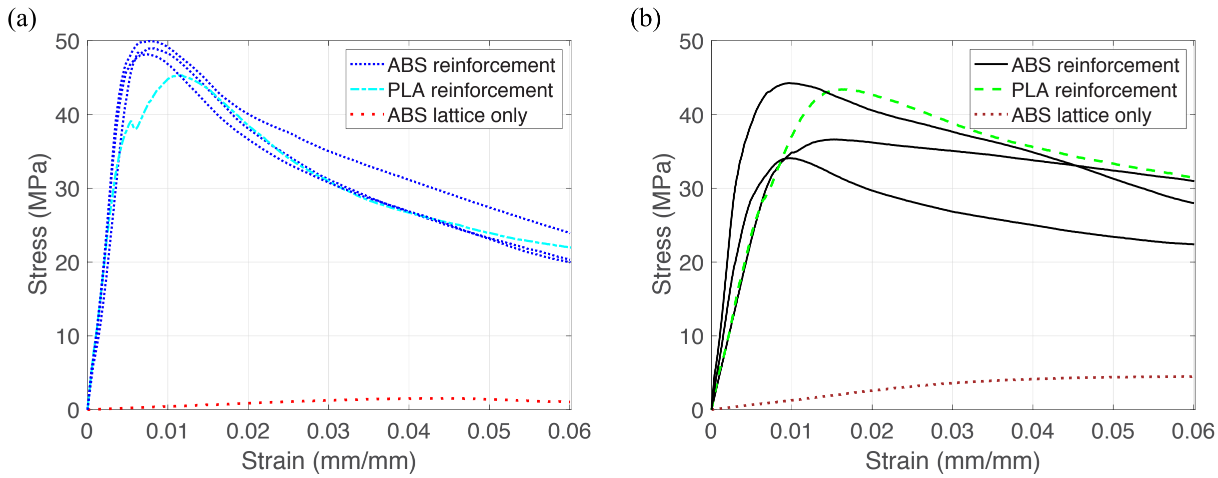

Figure 5 - Compressive stress-strain curves. The response of the pure lattice and the UHPC reinforced with PLA and ABS lattices is shown in (a) for 19.2% reinforcement and in (b) for 33.7% reinforcement.

3.2 Four-point bending results

The flexural results of the PLA lattice-reinforced UHPC specimens are summarized in Table 4. Note that all flexural specimens use PLA and not ABS, since PLA lattices do not require support structures to print at this scale, but ABS lattices would require the extra steps to dissolve the support material.

In these four-point bending tests, the 33.7% lattice-reinforced beams exhibit a higher peak load than the 19.2% lattice-reinforced beams. Both the 19.2% and 33.7% lattice-reinforced beams show high deflections at peak load and high toughness. The 95% confidence intervals for the mean toughness overlap for the 19.2% and 33.7% reinforcement ratios.

Table 4 – Four-point flexure results. Values indicate 95% confidence intervals of the mean.

Beam description	Peak load (kN)	Deflection at peak (mm)	Toughness (kN·mm)*
19.2% PLA lattice-reinforcement (N = 3)	14.6 ± 0.4	1.8 ± 0.4	17.5 ± 0.5
33.7% PLA lattice-reinforcement (N = 4)	20.1 ± 4.3	2.4 ± 0.6	17.5 ± 0.9
UHPC only (N = 1)	13.0	0.027	0.20
1.4% PLA fiber-reinforcement (N = 1)	6.6	0.021	0.10

N = Number of specimens
* Toughness at 1.52 mm midpoint deflection

The load–midpoint deflection curves of the flexural beams are shown in Figure 6. For midpoint deflections up to 1.52 mm (*i.e*. the span length divided by 150, as specified by [28]), all specimens behave similarly, independent of their reinforcing ratios (Figure 6a). The behavior differs at larger deflections, where the beams with a higher reinforcement ratio achieve higher loads (as shown in Figure 6b), which is opposite to the compression results. This difference in behavior at higher deflections is due to the increased crack growth resistance that a larger reinforcement ratio provides.

Similar to the compression results the beams with the higher reinforcement ratio exhibit a larger variability in their load–deflection curves due to the small openings of the 33.7% lattices that make the infiltration of UHPC less uniform. Figure 6b shows one 33.7% lattice-reinforced beam which underperforms compared to the other three samples; however, since its net deflection at peak load is not more than 1.5 interquartile ranges below the first quartile and it is not more than 1.5 interquartile ranges above the third quartile, we do not classify it as an outlier.

While all lattice-reinforced beams reveal high ductility, the beam reinforced with 1.4 vol% PLA fibers shown in Figure 6 by the red line exhibits very brittle behavior up to failure.

Hence, the highest volume fraction of fibers that could be incorporated into the UHPC mixture while maintaining a workable mix was not sufficient to provide any crack growth resistance. While the volume fractions of polymer fibers and printed reinforcement used in this work are very different (1.4 vol% fibers *vs* 19.2–33.7 vol% lattices), the results shown for PVA fiber reinforcement represent the best practically achievable option with this particular reinforcement approach and mortar composition.

The brittle performance of the plain UHPC beam agrees with the mechanical properties of a similar UHPC tested in [26]. In comparison to the unreinforced, UHPC-only beam, the lattice-reinforced beams are able to achieve higher flexural loads, since the reinforcement prevents a dominant crack from propagating through the beam.

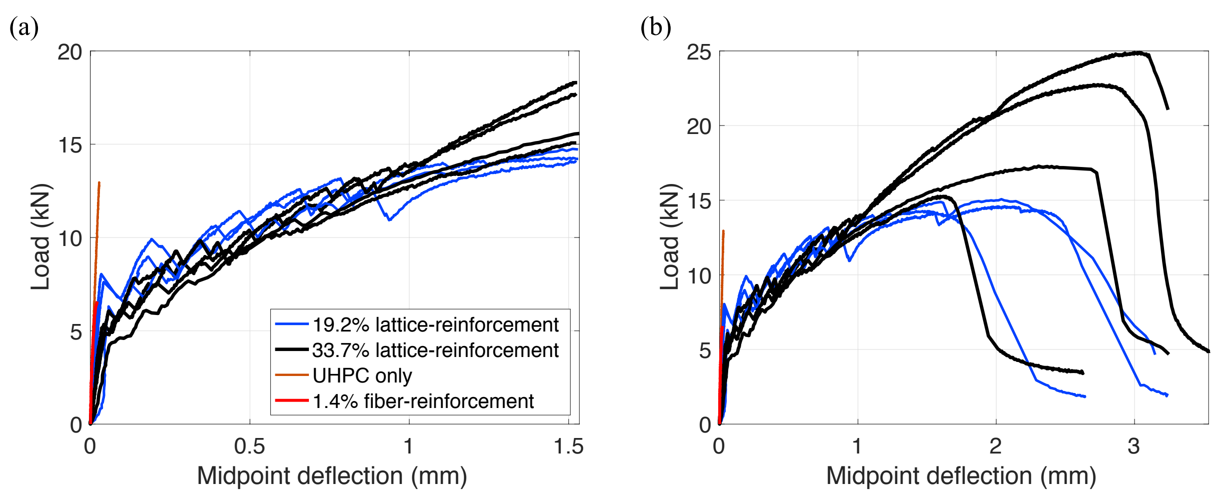

Figure 6 – Load–deflection curves for flexural specimens with varying amounts of polymeric reinforcement. The loading curve is plotted (a) until a maximum deflection of 1.52 mm (which was used for the toughness calculations in Table 4) and (b) until failure of the beams.

3.3 Failure characteristics

DIC software (OpteCAL) was utilized to investigate the sequence of crack initiation and crack pattern of a 19.2% lattice-reinforced beam during four-point bending. Figure 7 shows the strain field across the front face of the specimen. The strain field is then correlated with the load-deflection curve.

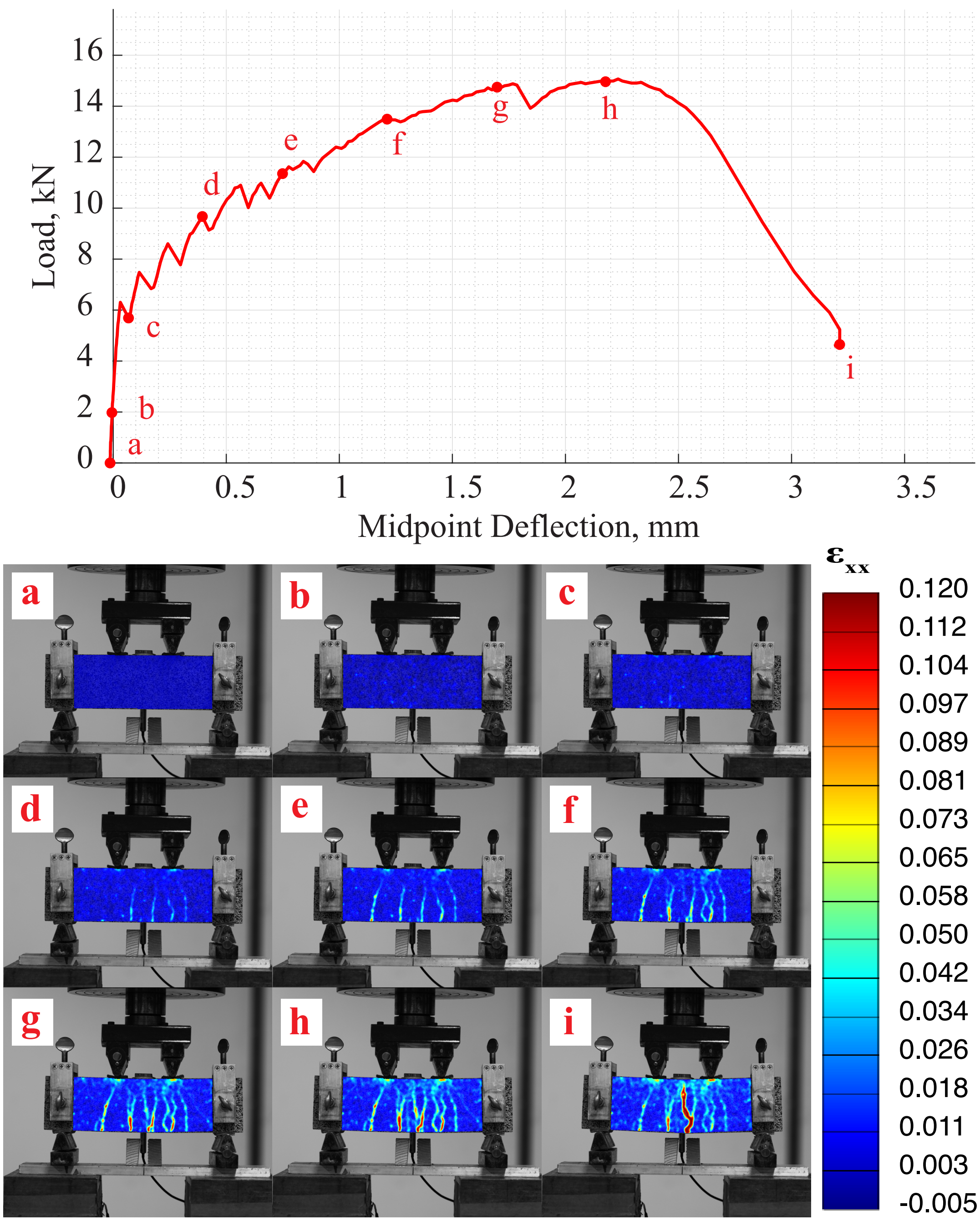

Figure 7 - Strain field across the front surface of flexural beams as measured with digital image correlation techniques. The progression of cracks is shown at various points across the load-deflection curve for the 19.2% lattice-reinforcement beam.

From (a) to (b), while the beam is in its elastic regime, no cracking could be observed. Hairline cracks initiate between (b) and (c), followed by multiple crack formation at (d). The multiple cracks increase in width from (d) to (f) in the tension zone while propagating towards the compression zone. Each of the multiple cracks continue to carry load, bifurcate and further increase in width between (g) and (h), which causes a flattening of the load–deflection curve. Eventually one of the multiple cracks becomes the dominant crack which leads to a drastic reduction in load capacity of the beam. The strain field of the specimen just prior to failure is shown in (i), with the dominant crack visible in red. DIC analysis for a 33.7% lattice-reinforced beam (not shown here) shows failure mechanism trends that are identical to the mechanisms exhibited by this 19.2% lattice-reinforced beam, with the 33.7% lattice-reinforced beam exhibiting a higher ultimate load.

Figure 8 contains images of representative fracture surfaces and side views of a 19.7% lattice-reinforced beam (Figure 8a, b), a 33.7% lattice-reinforced beam (Figure 8c, d), and the 1.4% fiber-reinforced beam (Figure 8e, f). Both lattice-reinforced beams reveal rough fracture surfaces which indicates that the cracks traveled through a tortuous path. This type of cracking contributes to the high ductility observed in these lattice-reinforced beams. The images of the lattice-reinforced beams also show step marks in the concrete, which are locations where the concrete debonded from the polymeric lattice, leading to high strain energy density values. The polymeric members show stress-whitening, indicating that they carried tensile stresses. Furthermore, the polymeric members' cup-and-cone fracture surfaces suggest that the fracture was ductile.

By contrast, the fiber-reinforced beams show smooth fracture surfaces, with no detectable fiber pull-out. This type of fracture surface is indicative of either a lack of debonding between the fibers and the matrix or inhomogeneous fiber distribution due to the low workability of the mix. Lattice-reinforcement has the advantage that it allows us to control precisely the distribution of the reinforcement within a structure.

Whereas in Salazar et al. [18], the polymeric lattice of the lattice-reinforced mortar samples fractured uniformly along a plane, the lattice-reinforced UHPC shown here does not have the polymeric members fracture along a single plane. The difference is due to the print direction, as previous research has shown that aligning the printed layers to be perpendicular to the crack plane results in increased tensile strength and fracture toughness [30,31]. The current work has the lattices printed in such a way that the build direction is aligned with the loading direction, as opposed to having the build and loading directions be orthogonal as in [18], which allowed the crack to cleave in-between printed layers.

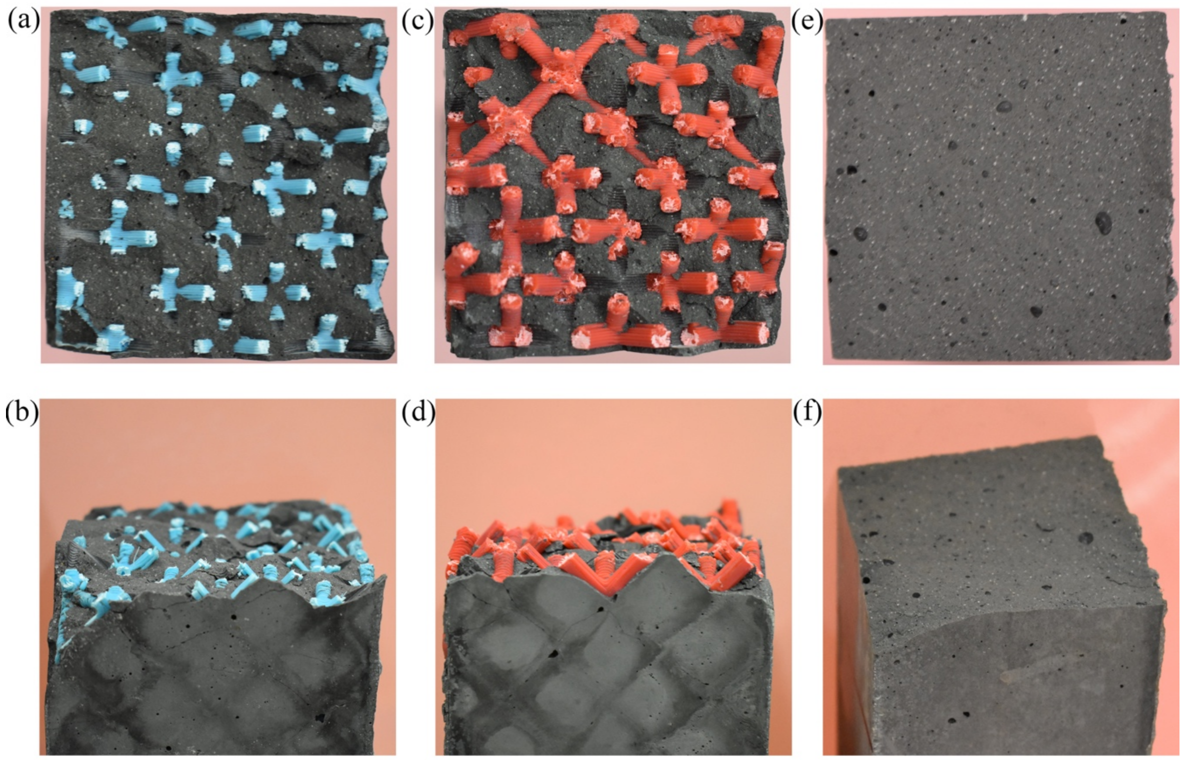

Figure 8 - Direct and side views of fracture surfaces of flexure specimens. (a) and (b) are representative of the 19.7% lattice-reinforced beams; (c) and (d) represent the 33.7% lattice-reinforced beams; (e) and (f) are the fiber-reinforced beam. Note that the dominant crack did not propagate through the entire beam, and beams were opened manually post-testing.

4. Conclusion

Lattice-reinforced concrete samples were created by fabricating polymeric lattices and infiltrating these lattices with ultra-high-performance concrete. These lattice-reinforced concrete samples exhibited high ductility in both compression and flexure. Compressive tests showed high strain density values, with the polymeric material choice (PLA or ABS) not having a significant effect. Increasing the percentage of the lattice reinforcement, however, led to a decrease and a higher variability in their compressive strength. Regarding flexure, all lattice-reinforced beams exhibited strain hardening up to peak load and the highest peak loads were observed with the higher lattice reinforcement of 33.7%. DIC was utilized to investigate the strain fields and to obtain information on the crack pattern during flexural loading. The results revealed multiple cracking and crack widening in these octet lattice-reinforced beams up to peak load.

While this paper focused on 3D-printed PLA and ABS octet lattice-reinforced structures as proofs of concept, the method itself is not limited to this specific kind of lattice geometry or to these particular polymeric materials. The ideal reinforcement geometry and material will depend on the application. Lattice reinforcement allows the placement of the reinforcement material to be controlled and hence optimized for specific loading scenarios — for example by increasing the volume fraction of reinforcement material in regions of higher expected tensile stress. Moreover, the optimal choice of polymeric material is a matter for future study, and the long-term stability of candidate polymers in contact with cementitious materials will need to be tested.

Fused deposition modeling 3D printing is known to be an anisotropic process, with 3D-printed components being stronger when loaded along extruded polymer filaments, and weaker when loaded across the interfaces between adjacent filaments. In this paper the specimens were printed such that the build direction was aligned with the flexural tests' loading direction. Therefore, the tension in the samples was predominantly aligned with the printed filaments. In this case, the cracks are forced to propagate through multiple printed layers, and not solely between layers. This approach allowed our specimens to reach as high a toughness as possible for the chosen manufacturing process.

The choice of 3D printing for lattice fabrication enabled rapid prototyping. Fabrication at larger scales and volumes — such as for building construction — could be accomplished by robotic extrusion printing with larger nozzles; the higher material deposition rates would substantially reduce production times. Indeed, the use of large-scale robotic extrusion printers in which individual extruded filaments of polymer are typically 5–10 mm in diameter would not only increase throughput but would also eliminate layering effects within the members of the printed lattices, since a single large extruded filament could serve as a complete member. If the member and unit cell sizes of these lattices were to be increased to aid high-volume production, while the materials remained similar, it can be anticipated that the basic failure mechanism would remain the same, although this would need to be confirmed through further experiments.

It may also be possible to develop injection-molding processes for geometrically regular reinforcement lattices. The octet lattice geometry is defined by approximately triangular, intersecting prismatic voids, so in principle a mold could be engineered with multiple retractable, interlocking cores to create the 3D lattice. While the development costs of such an approach would probably be very considerable, they may be warranted by the increased production rate. Layering and directional effects could also be minimized by molding rather than printing.

Acknowledgements

This research is supported by the National Research Foundation, Prime Minister’s Office, Singapore under its Campus for Research Excel- lence and Technological Enterprise (CREATE) programme. It was funded through a grant to the Berkeley Education Alliance for Research in Singapore (BEARS) for the Singapore-Berkeley Building Efficiency and Sustainability in the Tropics (SinBerBEST) Program. BEARS has been established by the University of California, Berkeley as a center for intel- lectual excellence in research and education in Singapore. We thank Chris Parsell, from UC Berkeley's Jacobs Institute for Design Innovation, for assistance with 3D printers. We also thank MiniFIBERS, Inc. for pro- viding PLA fibers.

Data Availability

The raw data required to reproduce these findings are available to download from http://dx.doi.org/10.17632/wv7hvgg8c7.1

References

[1] Bolander JE, Choi S. Fracture of fiber-reinforced cement composites : effects of fiber dispersion 2008:73–86. https://doi.org/10.1007/s10704-008-9269-4.

[2] Stähli P, Custer R, Van Mier JGM. On flow properties, fibre distribution, fibre orientation and flexural behaviour of FRC. Mater Struct Constr 2008;41:189–96. https://doi.org/10.1617/s11527-007-9229-x.

[3] Abrishambaf A, Barros JAO, Cunha VMCF. Relation between fibre distribution and post-cracking behaviour in steel fibre reinforced self-compacting concrete panels. Cem Concr Res 2013;51:57–66. https://doi.org/10.1016/j.cemconres.2013.04.009.

[4] Sarmiento E V., Geiker MR, Kanstad T. Influence of fibre distribution and orientation on the flexural behaviour of beams cast from flowable hybrid polymer-steel FRC. Constr Build Mater 2016;109:166–76. https://doi.org/10.1016/j.conbuildmat.2016.02.005.

[5] Zhou B, Uchida Y. Relationship between fiber orientation/distribution and post-cracking behaviour in ultra-high-performance fiber-reinforced concrete (UHPFRC). Cem Concr Compos 2017;83:66–75. https://doi.org/10.1016/j.cemconcomp.2017.07.007.

[6] Stähli P, van Mier JGM. Manufacturing, fibre anisotropy and fracture of hybrid fibre concrete. Eng Fract Mech 2007;74:223–42. https://doi.org/10.1016/j.engfracmech.2006.01.028.

[7] Švec O, Žirgulis G, Bolander JE, Stang H. Influence of formwork surface on the

orientation of steel fibres within self-compacting concrete and on the mechanical properties of cast structural elements. Cem Concr Compos 2014;50:60–72. https://doi.org/10.1016/j.cemconcomp.2013.12.002.

[8] Hegger J, Will N, Bruckermann O, Voss S. Load-bearing behaviour and simulation of textile reinforced concrete. Mater Struct Constr 2006;39:765–76. https://doi.org/10.1617/s11527-005-9039-y.

[9] Hegger J, Will N, Rüberg K. Textile reinforced concrete-A new composite material. Adv Constr Mater 2007 2007:147–56.

[10] Brückner A, Ortlepp R, Curbach M. Textile reinforced concrete for strengthening in bending and shear. Mater Struct Constr 2006;39:741–8. https://doi.org/10.1617/s11527-005-9027-2.

[11] Hegger J, Voss S. Investigations on the bearing behaviour and application potential of textile reinforced concrete 2008;30:2050–6. https://doi.org/10.1016/j.engstruct.2008.01.006.

[12] Schladitz F, Frenzel M, Ehlig D, Curbach M. Bending load capacity of reinforced concrete slabs strengthened with textile reinforced concrete. Eng Struct 2012;40:317–26. https://doi.org/10.1016/j.engstruct.2012.02.029.

[13] Vervloet J, Van Itterbeeck P, Verbruggen S, El Kadi M, De Munck M, Wastiels J, et al. Experimental investigation of the buckling behaviour of Textile Reinforced Cement sandwich panels with varying face thickness using Digital Image Correlation. Constr Build Mater 2019;194:24–31. https://doi.org/10.1016/j.conbuildmat.2018.11.015.

[14] Colombo IG, Colombo M, Prisco M. Bending behaviour of Textile Reinforced Concrete sandwich beams. Constr Build Mater 2015;95:675–85. https://doi.org/10.1016/j.conbuildmat.2015.07.169.

[15] Williams Portal N, Flansbjer M, Zandi K, Wlasak L, Malaga K. Bending behaviour of novel Textile Reinforced Concrete-foamed concrete (TRC-FC) sandwich elements. Compos Struct 2017;177:104–18. https://doi.org/10.1016/j.compstruct.2017.06.051.

[16] Deshpande VS, Fleck NA, Ashby MF. Effective properties of the octet-truss lattice material. J Mech Phys Solids 2001;49:1747–69. https://doi.org/10.1016/S0022-5096(01)00010-2.

[17] O'Masta MR, Dong L, St-Pierre L, Wadley HNG, Deshpande VS. The fracture toughness of octet-truss lattices. J Mech Phys Solids 2017;98:271–89. https://doi.org/10.1016/j.jmps.2016.09.009.

[18] Salazar B, Williams I, Aghdasi P, Ostertag C, Taylor H. International Congress on Polymers in Concrete (ICPIC 2018). Int Congr Polym Concr (ICPIC 2018) 2018:261–6. https://doi.org/10.1007/978-3-319-78175-4.

[19] Farina I, Fabbrocino F, Carpentieri G, Modano M, Amendola A, Goodall R, et al. On the reinforcement of cement mortars through 3D printed polymeric and metallic fibers. Compos Part B Eng 2016;90:76–85. https://doi.org/10.1016/j.compositesb.2015.12.006.

[20] Nam YJ, Hwang YK, Park JW, Lim YM. Feasibility study to control fiber distribution for enhancement of composite properties via three-dimensional printing. Mech Adv Mater Struct 2019;26:465–9. https://doi.org/10.1080/15376494.2018.1432809.

[21] Rosewitz JA, Choshali HA, Rahbar N. Bioinspired design of architected cement-polymer composites. Cem Concr Compos 2019;96:252–65. https://doi.org/10.1016/j.cemconcomp.2018.12.010.

[22] Xu Y, Šavija B. Development of strain hardening cementitious composite (SHCC) reinforced with 3D printed polymeric reinforcement: Mechanical properties. Compos Part B Eng 2019;174. https://doi.org/10.1016/j.compositesb.2019.107011.

[23] Aghdasi P. Development and Characterization of Green Ultra-High Performance Fiber-Reinforced Concrete (G-UHP-FRC) for Structural and Non-Structural Applications. University of California, Berkeley, 2019.

[24] Aghdasi P, Heid AE, Chao SH. Developing ultra-high-performance fiber-reinforced concrete for large-scale structural applications. ACI Mater J 2016;113:559–69. https://doi.org/10.14359/51689103.

[25] Aghdasi P, Ostertag CP. Green ultra-high performance fiber-reinforced concrete (G-UHP-FRC). Constr Build Mater 2018;190:246–54. https://doi.org/10.1016/j.conbuildmat.2018.09.111.

[26] Aghdasi P, Williams ID, Salazar B, Panditi N, Taylor HK, Ostertag CP. An Octet-Truss Engineered Concrete (OTEC) for lightweight structures. Compos Struct 2019;207:373–84. https://doi.org/10.1016/j.compstruct.2018.09.011.

[27] Branch Technology n.d. https://www.branch.technology (accessed July 17, 2020).

[28] ASTM C109/C109M-16a. Standard Test Method for Compressive Strength of Hydraulic Cement Mortars (Using 2-in. or [50-mm] Cube Specimens). ASTM Int 2016.

https://doi.org/10.1520/C0109.

[29] ASTM C1609/C1609M-19. Standard Test Method for Flexural Performance of Fiber-Reinforced Concrete (Using Beam With Third-Point Loading). ASTM Int 2005. https://doi.org/10.1520/C1609.

[30] Zou R, Xia Y, Liu S, Hu P, Hou W, Hu Q, et al. Isotropic and anisotropic elasticity and yielding of 3D printed material. Compos Part B Eng 2016;99:506–13. https://doi.org/10.1016/j.compositesb.2016.06.009.

[31] McLouth TD, Severino J V., Adams PM, Patel DN, Zaldivar RJ. The impact of print orientation and raster pattern on fracture toughness in additively manufactured ABS. Addit Manuf 2017;18:103–9. https://doi.org/10.1016/j.addma.2017.09.003.